Center for Turbulence Research
Proceedings of the Summer Program 2006

Toward the application of the impedance mismatch method to the expansion about incompressible flow acoustic equations

By R. Cohen†, A. Ooi† AND G. Iaccarino

This paper examines the different formulations available for performing Expansion about Incompressible Flow (EIF) acoustic simulations in which an incompressible flow calculation is split from the corresponding acoustic wave propagation problem. The relative merit of this approach is compared with fully compressible direct numerical simulation (DNS) and acoustic analogy. The Impedance Mismatch Method (IMM) for acoustic calculations is also discussed and its effectiveness for modelling curved geometry on a Cartesian grid is explored. In the literature, this method has never been applied to the problem of an unsteady non-uniform flow field. The objective of this work is to solve the EIF equations using the IMM Cartesian-based high order approach. The feasibility of achieving this is investigated using a number of test cases, the results of which indicate the difficulty of this approach from the standpoint of numerical stability and accuracy.

1. Introduction

The pioneering method of predicting aerodynamically generated sound was developed by Lighthill with his work on acoustic analogy theory (Lighthill 1952, 1954). In this approach, the compressible Navier–Stokes equations are rearranged into an inhomogeneous wave equation of the form

$$\frac{\partial^2 \rho}{\partial t^2} - a_\infty^2 \nabla^2 \rho = \frac{\partial^2 T_{ij}}{\partial x_i \partial x_j}, \tag{1.1}$$

where ρ is density, a_∞ is the speed of sound, and T_{ij} is Lighthill's stress tensor. The left-hand side represents acoustic wave propagation in a static homogeneous medium and the right-hand side represents quadrupole acoustic source terms. The assertion of the physical meaning of each part of this equation is the essence of the acoustic analogy theory. Later, Lilley produced an acoustic analogy that takes into account the mean flow refraction effect with a more complicated wave equation (Lilley 1974). To perform a numerical calculation using an acoustic analogy, a precise description of the near field is required to accurately obtain the source terms. This is done using numerical calculations or flow modelling. The wave operator is then inverted to determine the acoustic far field. The acoustic analogy approach has been popular with many variants in existence. It has been applied extensively to the problems of jet noise, fan noise, and trailing-edge noise.

Although it is a common approach for the generation and subsequent propagation of acoustic waves in fluids, acoustic analogy theory is not universally accepted (Fedorchenko 2000). It is somewhat arbitrary as to which flow variable to operate on (p or ρ), which terms to choose for the wave operator, and which to assign as source terms. Tam (2002)

† Department of Mechanical Engineering, The University of Melbourne

argues that without careful consideration, acoustic analogies can fail to identify physically meaningful acoustic sources.

Alternatively, aerodynamically generated sound may be calculated using direct numerical simulation (DNS) of the compressible governing equations. These equations unquestionably contain a more precise description of the physics. At low Mach numbers, DNS is challenging to perform because of the disparity in magnitudes in both the flow and acoustic quantities (Tam 1995). This requires numerical solvers with high order accurate discretisation schemes whose numerical errors are smaller than the acoustic quantities. Additionally, the length scale of the acoustic far field is many orders of magnitude larger than the near field. The time step requirement in the fine mesh of the near field is typically much smaller than the time step requirement of the far field. This means the calculation will be inefficient for the propagation of acoustic waves. These issues (and others) can lead to prohibitively expensive computational requirements for practical problems.

More recently with the advances in computational power, methods of directly calculating both the flow and acoustic fields using acoustic/viscous splitting techniques have been developed. These have a computational expense that is intermediate between acoustic analogies and fully compressible DNS and allow for the determination of the acoustic field from the near field out to the far field. These methods are detailed in the following section.

2. Expansion about incompressible flow

Expansion about Incompressible Flow (EIF) is a technique for determining aerodynamically generated acoustic fields for low Mach number flows. It involves first calculating the unsteady incompressible flow field, then using this information to drive a fully nonlinear acoustic calculation. The initial development of EIF (Hardin & Pope 1992, 1994) considered the decomposition of the flow variables

$$u_i = U_i + u_i', \tag{2.1}$$

$$p = P + p' \quad \text{and} \tag{2.2}$$

$$\rho = \rho_0 + \rho_1 + \rho', \tag{2.3}$$

where U_i, P, and ρ_0 are the hydrodynamic (incompressible flow) quantities; ρ_1 is a hydrodynamic density correction term; and u_i', p', and ρ' are acoustic fluctuations about their incompressible flow quantities. Using this decomposition, the incompressible Navier–Stokes equations may be subtracted from the compressible Navier–Stokes equations. If the viscous terms are neglected, these equations become

$$\frac{\partial \rho'}{\partial t} + \frac{\partial}{\partial x_i}((\rho_0+\rho_1)u_i' + \rho'(U_i+u_i')) = -\frac{\partial \rho_1}{\partial t} - U_i\frac{\partial \rho_1}{\partial x_i} \quad \text{and} \tag{2.4}$$

$$\begin{aligned}&\frac{\partial}{\partial t}((\rho_0+\rho_1)u_i' + \rho'(U_i+u_i')) \\ &+\frac{\partial}{\partial x_j}\left[((\rho_0+\rho_1)u_i' + \rho'(U_i+u_i'))(U_j+u_j') + (\rho_0+\rho_1)U_i u_j' + p'\delta_{ij}\right] \\ &= -\frac{\partial}{\partial t}(\rho_1 U_i) - U_j\frac{\partial}{\partial x_j}(\rho_1 U_i).\end{aligned} \tag{2.5}$$

Hardin and Pope argued that no flow is truly incompressible and there must be a (small) incompressible density fluctuation to balance the incompressible pressure fluctuations.

These hydrodynamic density fluctuations may be relatively large as compared to the acoustic density fluctuations. Hardin and Pope proposed that the hydrodynamic density correction may be calculated from

$$\overline{P}(x_i) = \lim_{T\to\infty} \frac{1}{T}\int_0^T P(x_i,t)dt, \tag{2.6}$$

$$p_1(x_i,T) = P(x_i,t) - \overline{P}(x_i) \quad \text{and} \tag{2.7}$$

$$\rho_1(x_i,t) = \frac{1}{c^2} p_1(x_i,t). \tag{2.8}$$

To close this set of equations, the fluctuations about the incompressible flow are assumed isentropic and the relationship between acoustic pressure p' and acoustic density ρ' becomes

$$\frac{\partial p'}{\partial t} - c^2 \frac{\partial \rho'}{\partial t} = c^2 \frac{\partial \rho_1}{\partial t}, \tag{2.9}$$

where the speed of sound is given by the relation

$$c^2 = \frac{\gamma p}{\rho} = \frac{\gamma(P+p)}{\rho_0 + \rho_1 + \rho'}. \tag{2.10}$$

Initial validation of this technique was performed on a pulsating and an oscillating sphere. Hardin and Pope's technique was later criticised (Shen & Sorensen 1999a) for being inconsistent and that the inclusion of the hydrodynamic density correction does not include any new information. Rearranging the equations can show that there is no source term present, meaning only the trivial solution should be obtained. Rather than Eq. (2.9), Hardin and Pope's simulations actually use the isentropic relation

$$p/p_0 = (\rho/\rho_0)^\gamma, \tag{2.11}$$

which may be shown to correspond to the equation

$$\frac{\partial p'}{\partial t} - c^2 \frac{\partial \rho'}{\partial t} = c^2 \frac{\partial \rho_1}{\partial t} - \frac{\partial P}{\partial t}, \tag{2.12}$$

which contains a source term $\partial P/\partial t$ from the incompressible flow. An equivalent but simpler formulation was given (Shen & Sorensen 1999b) where the flow variables are decomposed by

$$u_i = U_i + u_i', \tag{2.13}$$

$$p = P + p' \quad \text{and} \tag{2.14}$$

$$\rho = \rho_0 + \rho'. \tag{2.15}$$

The acoustic equations are given by

$$\frac{\partial \rho'}{\partial t} + \frac{\partial}{\partial x_i}((\rho_0+\rho')u_i' + \rho' U_i) = 0, \tag{2.16}$$

$$\begin{aligned}&\frac{\partial}{\partial t}((\rho_0+\rho')u_i' + \rho' U_i)\\ &+\frac{\partial}{\partial x_j}\left[((\rho_0+\rho')u_i' + \rho' U_i)(U_j+u_j') + \rho_0 U_i u_j' + p'\delta_{ij}\right] = 0 \quad \text{and}\end{aligned} \tag{2.17}$$

$$\frac{\partial p'}{\partial t} - c^2 \frac{\partial \rho'}{\partial t} = -\frac{\partial P}{\partial t}. \tag{2.18}$$

This formulation was validated by simulating the acoustic field generated by a pulsating sphere and also by the laminar wake behind a circular cylinder.

A more rigorous derivation of the EIF equations was given by Slimon, *et al.* (2000). They sought a physical interpretation of the various terms in the EIF equations as well as their inherent assumptions and limitations. To do so, they performed a Janzen Rayleigh expansion, where each of the flow variables is expanded as a power series in $\varepsilon^2 = \gamma M^2$. The decomposition is

$$p = p_0 + \varepsilon^2\overline{p}_1 + \varepsilon^4\overline{p}_2 + \varepsilon^6\overline{p}_3 + \ldots = p_0 + p_1 + p_2 + p_3 + \ldots \quad , \tag{2.19}$$

$$\rho = \rho_0 + \varepsilon^2\overline{\rho}_1 + \varepsilon^4\overline{\rho}_2 + \varepsilon^6\overline{\rho}_3 + \ldots = \rho_0 + \rho_1 + \rho_2 + \rho_3 + \ldots \quad , \tag{2.20}$$

$$u_i = u_{i0} + \varepsilon^2\overline{u}_{i1} + \varepsilon^4\overline{u}_{i2} + \varepsilon^6\overline{u}_{i3} + \ldots = u_{0i} + u_{1i} + u_{2i} + u_{3i} + \ldots \quad , \quad \text{and} \tag{2.21}$$

$$T = T_0 + \varepsilon^2\overline{T}_1 + \varepsilon^4\overline{T}_2 + \varepsilon^6\overline{T}_3 + \ldots = T_0 + T_1 + T_2 + T_3 + \ldots \quad . \tag{2.22}$$

These variables are substituted into the compressible continuity, momentum, and energy equations as well as an equation of state. Equating the lowest order coefficients (ε^{-2}) yields the zeroth-order equations that govern the thermodynamic field (p_0, ρ_0, T_0). Equating the ε^0 coefficients yields the first-order equations that govern the hydrodynamic field (p_1, ρ_1, u_{0i}, T_1). Finally, equating the ε^2 terms produces the second-order equations that govern the compressible field ($p_2, \rho_2, u_{1,i}, T_2$). Higher order terms only become significant at high Mach numbers.

By assuming a fixed thermodynamic field, one may recover the incompressible momentum and continuity equations from the first-order equations. The Hardin and Pope EIF momentum and continuity equations may be recovered from this Mach number expansion approach by combining second-order and higher equations while neglecting the viscous terms. The EIF acoustic perturbation quantities are then defined as

$$\rho' = \sum_{m=2}^{\infty} \varepsilon^{2m}\overline{\rho}_m, \tag{2.23}$$

$$u_i' = \sum_{m=2}^{\infty} \varepsilon^{2m}\overline{u}_{mi} \quad \text{and} \tag{2.24}$$

$$p' = \sum_{m=2}^{\infty} \varepsilon^{2m}\overline{p}_m. \tag{2.25}$$

By combining the zeroth-order and higher energy equations and equations of state while neglecting viscous effects, one may derive the final equation required to close this set

$$\frac{Dp'}{Dt} - \gamma\frac{D\rho'}{Dt} - \gamma\frac{D\Pi_n}{Dt} = 0, \tag{2.26}$$

where Π_n is a function of ρ_1 and ρ'. This is equivalent to the isentropic relation $p = \rho^\gamma$. The Slimon equations were applied to the problem of sound generated by a spinning vortex pair. Data from numerical simulations show good agreement with the analytical solution. The complete set of equations are (Slimon, *et al.* 1999)

$$\frac{\partial\rho'}{\partial t} + \frac{\partial}{\partial x_i}\left[(1+\rho_1+\rho')u_i' + \rho' U_i\right] = -\frac{\partial\rho_1}{\partial t} - U_i\frac{\partial\rho_1}{\partial x_i}, \tag{2.27}$$

$$\begin{aligned}&\frac{\partial}{\partial t}\left[(1+\rho_1+\rho')u_i' + \rho' U_i\right] + \frac{\partial}{\partial x_j}\left[(1+\rho_1)(U_i u_j' + U_j u_i' + u_i' u_j')\right] \\ &+\frac{\partial}{\partial x_j}\left[\rho'(U_i U_j + U_i u_j' + U_j u_i' + u_i' u_j')\right] + \frac{\partial p'}{\partial x_i} = -\frac{\partial(\rho_1 U_i)}{\partial t} - \frac{\partial(\rho_1 U_i U_j)}{\partial x_j},\end{aligned} \tag{2.28}$$

$$\frac{D\rho_1}{Dt} = M^2 \frac{DP}{Dt}, \quad \text{and} \tag{2.29}$$

$$\frac{D\rho'}{DT} = M^2 \frac{Dp'}{Dt} - \left(\frac{\gamma - 1}{2}\right) \frac{D\left(\rho_1^2\right)}{Dt}. \tag{2.30}$$

The EIF equations described so far do not include viscous terms. Seo and Moon (2003) retain the viscous stresses and heat flux terms in their EIF formulation. Generally they are able to obtain more accurate solutions than for the simpler EIF formulations previously discussed.

3. Impedance mismatch method

The Impedance Mismatch Method (IMM) is a technique for modelling solid wall boundaries in acoustic simulations that obviates the need for a body fitted grid. A curved geometry is described on a Cartesian grid by the assignment of characteristic density values at each grid point. Fluid regions and solid wall regions are assigned different values for their characteristic density. The speed of sound is assumed to be the same in the non-physical solid wall region as in the fluid region. This treatment causes incoming acoustic waves to be reflected at the interface of the mismatched impedances (ρa) as though they had encountered a solid wall boundary. Initially developed by Chung and Morris (1998), the IMM is typically applied to the linearised Euler equations.

The development of the IMM proceeds as follows. The one-dimensional linearised Euler equations with no mean flow are

$$\frac{\partial \rho}{\partial t} + \rho_0 \frac{\partial u}{\partial x} = 0, \tag{3.1}$$

$$\frac{\partial u}{\partial t} + \frac{1}{\rho_0} \frac{\partial p}{\partial x} = 0, \quad \text{and} \tag{3.2}$$

$$\frac{\partial p}{\partial t} + \rho_0 a_0^2 \frac{\partial u}{\partial x} = 0. \tag{3.3}$$

The time derivatives are supposed to be continuous functions of x. The terms inside the spatial derivatives and the ρ_0 coefficients of the spatial derivatives are only piecewise continuous because of the discontinuity at the interface. However, the product of these terms are continuous. In order to match the discontinuity and to have a smooth function for the spatial derivative operator to apply to, the equations are modified to be

$$\frac{\partial \rho}{\partial t} + \frac{\partial (u\rho_0)}{\partial x} = 0, \tag{3.4}$$

$$\frac{\partial u}{\partial t} + \frac{\partial (p/\rho_0)}{\partial x} = 0, \quad \text{and} \tag{3.5}$$

$$\frac{\partial p}{\partial t} + \frac{\partial (u\rho_0)}{\partial x} = 0. \tag{3.6}$$

In these equations the speed of sound (a_0) has been assumed to be unity. The characteristic density in the fluid region is also set to unity while in the solid wall regions it is given the recommended value (for numerical stability) of 1/30. This smaller density in the solid wall region is to ensure that acoustic waves are reflected with the correct phase. The amplitude of the reflected waves may be shown to be

$$|p_r/p_i| = \frac{1/\rho_2 - 1}{1/\rho_2 + 1}. \tag{3.7}$$

The one-dimensional IMM equations previously given are identical to the linearised Euler equations far away from the wall and produce the effect of a solid wall in the vicinity of the interface.

The full three-dimensional linearised Euler equations with mean flow Mach number M in the x-direction are given by

$$\frac{\partial}{\partial t}\begin{bmatrix}\rho\\ u\\ v\\ w\\ p\end{bmatrix}+\frac{\partial}{\partial x}\begin{bmatrix}M\rho+\rho_0 u\\ Mu+p/\rho_0\\ Mv\\ Mw\\ Mp+\rho_0 u\end{bmatrix}+\frac{\partial}{\partial y}\begin{bmatrix}\rho v\\ 0\\ p/\rho_0\\ 0\\ \rho_0 v\end{bmatrix}+\frac{\partial}{\partial z}\begin{bmatrix}\rho_0 w\\ 0\\ 0\\ p/\rho_0\\ \rho_0 w\end{bmatrix}=\begin{bmatrix}0\\ 0\\ 0\\ 0\\ S\end{bmatrix}. \tag{3.8}$$

Chung and Morris demonstrated the effectiveness of the IMM by considering scattering off several two- and three-dimensional bodies in a stationary flow.

Laik and Morris (2000) later developed an IMM formulation where flow variables were decomposed into three parts: an unperturbed flow, a known incident perturbation, and the undetermined scattered perturbation. The source terms in the scattered field equations comes from the difference between the incident field in a uniform flow in the absence of the body and the non-uniform flow in the presence of the body. The physical basis for this is unclear. Despite this, Laik and Morris were able to obtain good agreement with analytical solution for the acoustic scattering from a cylinder, Rankine oval, and a sphere in a fluid at rest. Simulations involving a steady non-uniform flowfield were also performed.

3.1. *Stability analysis of the impedance mismatch method*

A stability analysis of the Impedance Mismatch Method is performed by considering the IMM version of the linearised Euler equations in one-dimension given by Eq. (3.4)–(3.5). Using explicit finite difference schemes, these may be discretised into a system of equations of the form

$$\frac{\partial \vec{x}}{\partial t} = A\vec{x}, \tag{3.9}$$

where A is a matrix of constant coefficients. The eigenvalues of this matrix determine the stability requirements of the numerical timestepping scheme. The domain considered is a 100-point equispaced periodic grid of which 50% is fluid region and 50% is solid wall region.

The analysis reveals that only purely imaginary eigenvalues are obtained. Figures 1(a) and (b) both show that as the wall density ρ_0 is decreased, the system will have a larger maximum eigenvalue and will be less stable. This explains why Chung and Morris (1998) recommend using a modest value of $1/30$ for ρ_0 which is a reasonable balance between numerical stability and reflected wave amplitude. Figure 1(a) shows that smoothing the ρ_0 transition at the wall boundary may make the computation more stable. Perhaps this is why less spurious waves are generated for walls that have a smoother interface. Finally, Fig. 1(b) shows that as the stencil size of the finite difference scheme is increased, the calculation becomes less stable.

4. Governing equations, numerical methods, and test cases

In order to make the application of the IMM simpler, the Shen and Sorensen equations (Eq. (2.16)–(2.18)) are linearised. For low Mach number problems ($M \leq 0.2$), this is

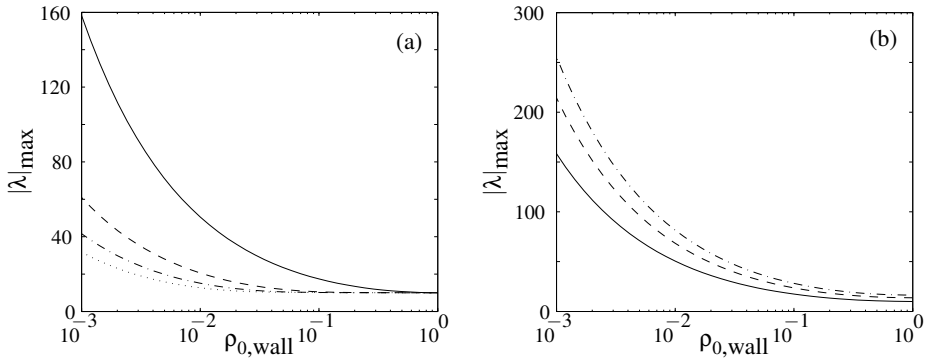

FIGURE 1. Maximum eigenvalue magnitude as a function of wall density. Plot (a) shows curves for interface smoothing over different numbers of points; 0 (———), 3 (– – – –), 5 (—·—), and 7 (·····). Plot (b) shows curves for centred finite difference schemes of order 2 (———), 4 (– – – –), and DRP4 (—·—).

Case	Dimensions	Description	Problem Layout	Acoustic Sources	Flow Field
1	1D	infinite wall	Fig. 2(a)	initial pulse	static
2	1D	finite wall	Fig. 2(b)	initial pulse	static
3	2D	1 cylinder	Fig. 3(a)	time periodic	static
4	2D	3 cylinders	Fig. 3(b)	time periodic	static
5	2D	1 cylinder	–	time periodic	steady non-uniform
6	2D	1 cylinder	–	unsteady incompressible flow	$Re = 150$, $M = 0.2$

TABLE 1. Summary of test cases

acceptable because the perturbation terms are small. Dropping all products of the small perturbations produces

$$\frac{\partial \rho'}{\partial t} + \underbrace{\frac{\partial}{\partial x_i}(\rho_0 u_i')}_{\text{term 1}} + \underbrace{\frac{\partial}{\partial x_i}(\rho' U_i)}_{\text{term 2}} = 0, \tag{4.1}$$

$$\frac{\partial}{\partial t}(\rho_0 u_i' + \rho' U_i) + \underbrace{\frac{\partial}{\partial x_j}(\rho_0 U_i u_j' + \rho_0 u_i' U_j + \rho' U_i U_j)}_{\text{term 3}} + \underbrace{\rho_0 \frac{\partial}{\partial x_i}(p'/\rho_0)}_{\text{term 4}} = 0 \quad \text{and} \tag{4.2}$$

$$\frac{\partial p'}{\partial t} - c^2 \frac{\partial \rho'}{\partial t} = -\frac{\partial P}{\partial t}. \tag{4.3}$$

Terms 1 and 4 will be calculated using centered finite difference stencils, even across the interfaces of solid wall regions. Terms 2 and 3 are convection terms that will be assumed zero inside solid wall regions, while in fluid regions their finite difference stencils will be such that they never cross into the solid wall region.

Numerical time-stepping of the EIF equations is carried out using the standard fourth-order explicit Runge–Kutta technique. Seven-point stencil spatial derivatives are taken using dispersion relation preserving (DRP) finite difference schemes from Tam (1995). To reduce the impact of spurious waves generated at the sharp interfaces, filtering of the solution is to be performed between timesteps. The optimised explicit coefficients are

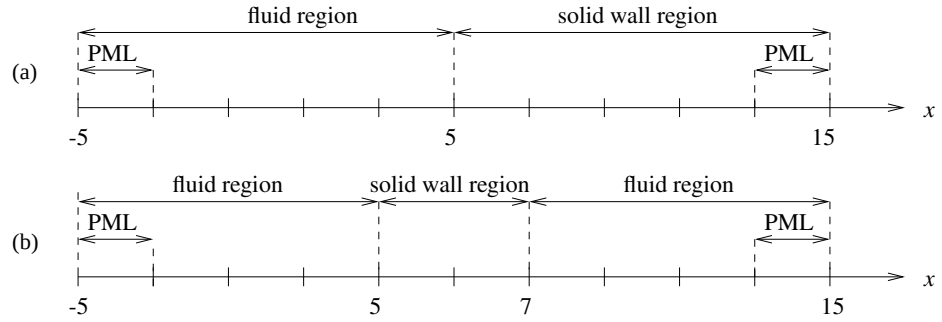

FIGURE 2. One-dimensional domains for cases 1 (a) and cases 2 (b)

taken from Bogey and Bailly (2004). Acoustic waves radiating out of the computational domain are absorbed by using a Perfectly Matched Layer (PML) of Hu (2002) in unsplit physical variables.

The validation of the numerical approach is to proceed in an incremental manner. Firstly, one-dimensional acoustic scattering from a solid region will be considered. This will be followed by acoustic scattering in two dimensions. The solver will then be run with a steady non-uniform mean flow to see its effect. Finally, a full test using unsteady laminar flow data and source terms calculated from the incompressible flow will be carried out. All of the acoustic problems to be considered are linear. This is reasonable considering that the ultimate cylinder test case will be a laminar low Mach number problem, which is inherently linear. Table 1 shows a summary of the test cases.

In case 1 the domain is initialised with the Gaussian pressure pulse given by

$$p = 0.001 \exp\left[-\ln\left(x^2/0.2^2\right)\right]. \tag{4.4}$$

The effect of different amounts of ρ_0 interface smoothing using a cosine function is to be investigated in this case. Unless otherwise indicated, numerical filtering will not be applied in these simulations.

In case 2 the domain is initialised with the same field as case 1. This case investigates the amount of sound transmitted through a finite solid wall region. A method of eliminating the impact of these waves is investigated.

Case 3 is a single cylinder linear acoustic wave scattering problem taken from Tam and Hardin (1997). A time periodic acoustic source is located near the cylinder and is given by the equation

$$\frac{\partial P}{\partial t} = 0.001 \exp\left[-\ln\left(((x-a)^2+y^2)/0.2^2\right)\right] \sin(8\pi t), \tag{4.5}$$

with $a = 4$. Case 4 is a three cylinder acoustic scattering test problem taken from Dahl (2004). The same high frequency source is used as case 3, but with $a = 0$. This case is a more rigorous test of the nearfield accuracy of the numerical method.

Case 5 tests the numerical approach on a non-uniform steady flow, the scattering of a cylinder in cross flow. A two-dimensional, inviscid, and incompressible (potential) flow around a cylinder in polar coordinates $[r, \theta]$ can be described as

$$U_r = \left(1 - \frac{R^2}{r^2}\right) M \cos\theta \quad \text{and} \tag{4.6}$$

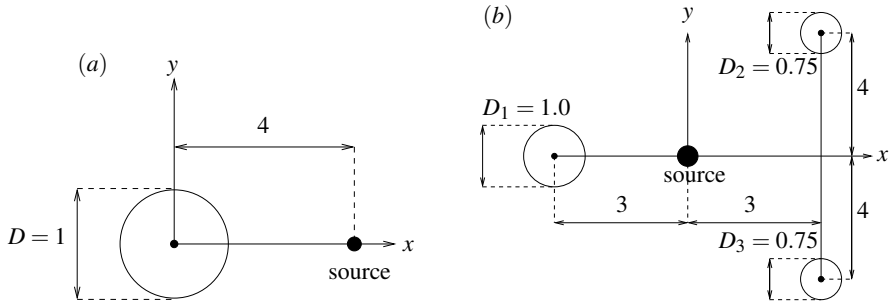

FIGURE 3. Scattering test problem layouts (a) Single cylinder problem (b) Three cylinder problem

$$U_\theta = -\left(1+\frac{R^2}{r^2}\right) M \sin\theta, \tag{4.7}$$

where U_∞ is the free stream velocity and R is the radius of the cylinder. This is the first test of the convective terms of the EIF equations. It is also a test of the effectiveness and stability attributes of the one-sided stencil scheme near the body. Two time periodic monopoles are placed on the rear surface of the cylinder to resemble a realistic flow induced acoustics calculation.

Test case 6 is a comprehensive test of the technique. In this simulation, the flowfield is obtained from an flow calculation performed using an unstructured incompressible-fluid solver for LES/DNS (Mahesh *et al.* 2004, Ham & Iaccarino 2004) at $Re = 150$ and $M = 0.2$. This solution also supplies the acoustic source terms. This case tests the entire solution procedure from the governing equations to the numerical method. It also tests the effectiveness of IMM for source terms that are in the vicinity of the body surface.

5. Results

5.1. *Case 1 - 1D relected wave*

This calculation was run using different amounts of ρ_0 interface smoothing. Figure 4(a) shows the time history of acoustic pressure at $x = -3$ when the reflected wave is passing by this location. For the sharp interface case, spurious waves that propagate at non-physical speeds are generated when the pulse strikes the interface. These are suppressed in all other cases. The amplitude of the reflected wave is slightly reduced in the cases of the sharp and smoothed interfaces. In the sharp interface filtered solution, the amplitude of the wave more closely matches the reference solution.

5.2. *Cases 2 - 1D transmitted wave*

The results for this test case are shown in Fig. 5. An acoustic wave that is transmitted into the solid wall region is seen to periodically contaminate the solution both in front and behind the body. This effect is eliminated by the addition of PML-type damping inside the solid wall region. Using such a technique is reliant on having a body that is thick enough to have an effective absorbing region as in this case.

5.3. *Cases 3 and 4 - 2D single and multiple cylinder scattering*

The results of these test cases are shown in Figs. 6 and 7. IMM is seen to do an effective job of modelling the curved geometry of the cylinders. The accuracy of IMM for linear scattering problems in a static environment is verified.

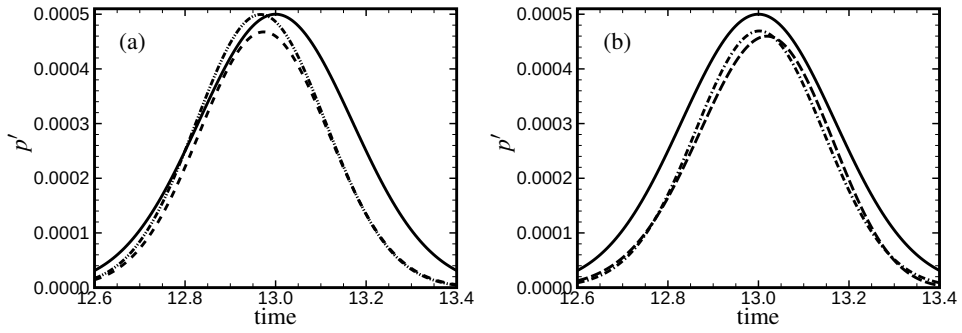

FIGURE 4. Probe time history at $x = -3$ for case 1. Reference solution (———), sharp interface (– – – –), sharp interface with numerical filtering (—··—), 3-point smoothed interface (—·—), 7-point smoothed interface (— — —).

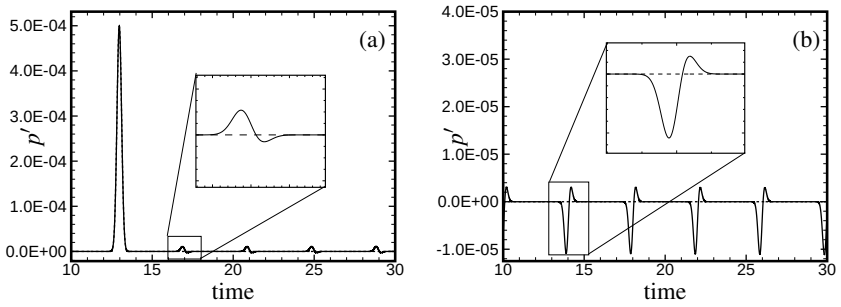

FIGURE 5. Case 3 acoustic pressure time histories at $x = -3$ (a) and $x = 10$ (b). The simulation is run without (———) and with (– – – –) damping inside the solid wall region

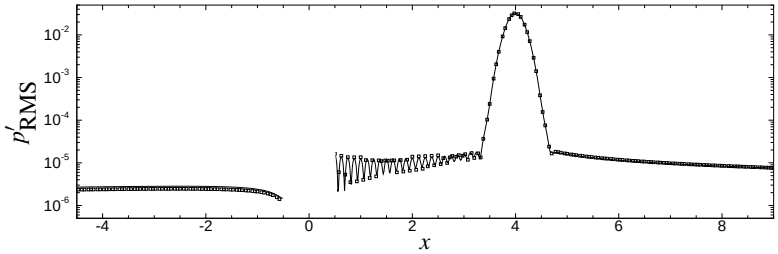

FIGURE 6. Case 3 RMS profile of p' along the x-axis for the analytical solution (———) and the numerical solution using $\Delta x = 0.025$ (□)

5.4. *Case 5 - 2D single cylinder scattering in a non-uniform potential flow field*

An instantaneous contour plot for this test case is shown in Fig. 8. This is primarily a test of the stability of this approach, as there is no analytical solution available for this test case.

5.5. *Case 6 - single cylinder, $Re = 150$, $M = 0.2$, flow induced acoustic scattering*

This case is a complete test of the technique that uses data from an incompressible flow calculation. Many different combinations of EIF formulations, one/two-sided stenciling

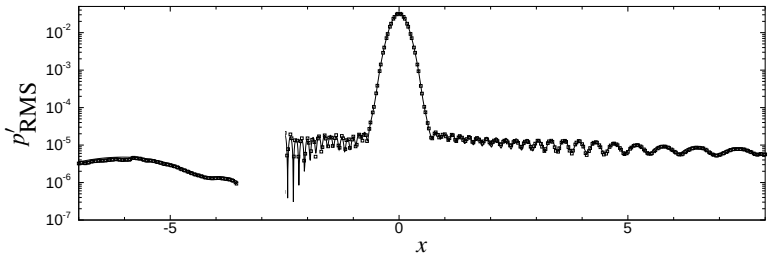

FIGURE 7. Case 4 RMS profile of p' along the x-axis for the analytical solution (———) and the numerical solution using $\Delta x = 0.025$ (□)

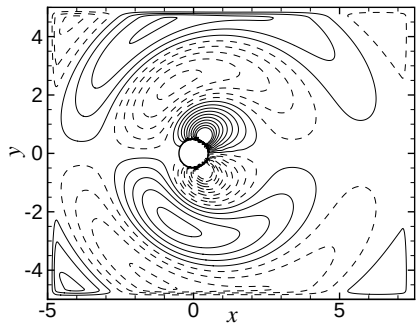

FIGURE 8. Case 5 instantaneous contours of acoustic pressure at time $t = 32$. The 20 contour levels equispaced from 10^{-4} to -10^{-4} with dashed lines indicating negative sign

at the interface, ρ_0 interface smoothing, finite difference schemes, filters, timesteps, grid densities, and cylinder damping techniques have been attempted. The formulation given in the paper appears to be the most stable. The main limitation of the current technique is the computational inefficiency of using a stretched Cartesian grid to cover the required domain. This test case remains part of ongoing work. If successful, the approach should be extended to a multi-block grid for improved efficiency.

6. Conclusions

In this paper the merits of various EIF formulations were discussed in relation to each other and in the larger context of acoustic prediction methods, including acoustic analogies and direct numerical simulation. In the literature IMM is seen to be a promising method of performing complex geometry acoustic scattering problems on a Cartesian grid.

Application of the IMM to EIF was seen to be effective for static media. The introduction of non-uniform flows introduces the difficulty of how to handle convective terms in the vicinity of the interface. The stability and accuracy of reflections for acoustic sources in the near vicinity of an interface is also an open question. During this investigation, a formulation that could be made stable in a steady non-uniform flow test case was determined. These initial computations are encouraging, but the approach is yet to be proved for a realistic, unsteady flow field.

Acknowledgments

This project is partially supported by the Maritime Platforms Division (MPD) of the Defense, Science and Technology Organisation (DSTO) of Australia. The Victorian Partnership for Advanced Computing (VPAC) are also gratefully acknowledged for their supply of computing resources.

REFERENCES

Bogey, C. & Bailly, C. 2004 A family of low dispersive and low dissipative explicit schemes for flow and noise computations *J. Comp. Phys.* **194**, 194–214.

Chung, C. & Morris, P. J. 1998 Acoustic Scattering From Two- and Three-Dimensional Bodies *J. Comput. Acoust.* **6**, 357–375.

Dahl, M. D. 2004 Fourth Computational Aeroacoustics (CAA) Workshop on Benchmark Problems *NASA/CP–2004-213954*.

Fedorchenko, A. T. 2000 On Some Fundamental Flaws In Present Aeroacoustic Theory *J. Sound Vibr.* **232**, 719–782.

Ham, F. & Iaccarino, G. 2004 Energy conservation in collocated discretization schemes on unstructured meshes *Center for Turbulence Research Annual Research Briefs 2004*, 3–14.

Hardin, J. & Pope, D. S. 1992 A new technique for aerodynamic noise calculation *14th DGLR/AIAA Aeroacoustics Conference*.

Hardin, J. & Pope, D. S. 1994 An Acoustic/Viscous Splitting Technique for Computational Aeroacoustics *Theoret. Comput. Fluid Dyn.* **6**, 323–340.

Hu, F. Q. 2002 On Constructing Stable Perfectly Matched Layers as an Absorbing Boundary Condition for Euler Equations *AIAA Paper 2002-0227*.

Laik, O. A. & Morris, R. J. 2000 Direct Simulation of Acoustic Scattering by Two- and Three-Dimensional Bodies *J. Aircraft* **37**, 68–75.

Lighthill, M. J. 1952 On Sound Generated Aerodynamically: I. General Theory *Proc. Roy. Soc. London Ser. A.* **211**, 564–581.

Lighthill, M. J. 1954 On Sound Generated Aerodynamically: II. Turbulence as a source of sound *Proc. Roy. Soc. London Ser. A.* **222**, 1–32.

Lilley, G. M. 1974 On the Nouse From Jets *Noise Mechanisms, AGRAD-CP-131*, 13.1–13.12.

Mahesh, K., Constantinescu, G. & Moin, P. 2004 A numerical method for large-eddy simulation in complex geometries *J. Comp. Phys.* **197**, 215–240.

Moon, Y. J., Seo, J. H., Koh, S. R. & Cho, Y. 2003 Aeroacoustic tonal noise prediction of open cavity flows involving feedback *Comput. Mech.* **31**, 359–366.

Seo, J. H. & Moon, Y. J. 2003 A hybrid method for prediction of aeroacoustic noise of wall-bounded shear flows at low Mach numbers *AIAA Paper 03-3270*.

Shen, W. Z. & Sorensen, J. 1999a Aeroacoustic Modelling of Low-Speed Flows *Theoret. Comput. Fluid Dyn.* **13**, 271–289.

Shen, W. Z. & Sorensen, J. 1999b Comment on the Aeroacoustic Formulation of Hardin and Pope *AIAA J.* **37**, 141–143.

Slimon, S. A., Soteriou, M. C. & Davis, D. W. 1999 Computational Aeroacoustics Simulations Using the Expansion About Incompressible Flow Approach *AIAA J.* **37**, 409–416.

Slimon, S. A., Soteriou, M. C. & Davis, D. W. 2000 Development of Computa-

tional Aeroacoustics Equations for Subsonic Flows Using a Mach Number Expansion Approach *J. Comp. Phys.* **159**, 377–406.

Tam, C. K. W. 1995 Computational Aeroacoustics: Issues and Methods *AIAA J.* **33**, 1788–1796.

Tam, C. K. W. 2002 Computational Aeroacoustics Examples Showing the Failure of the Acoustic Analogy Theory to Identify the Correct Noise Sources *J. Comput. Acoust.* **10**, 387–405.

Tam, C. K. W. & Hardin, J. C. 1997 Second Computational Aeroacoustics (CAA) Workshop on Benchmark Problems *NASA Conference Publication 3552*.